

Passive stabilization of isometric contractions in skeletal muscles

Hudson Borja da Rocha^{1,*} and Lev Truskinovsky^{2,†}

¹*CIRB, CNRS UMR 7241, INSERM U1050, Collège de France and PSL Research University, F-75005 Paris, France*

²*PMMH, CNRS-UMR 7636 PSL-ESPCI, 10 Rue Vauquelin, 75005 Paris, France*

(Dated: April 2, 2022)

The passive transient response of tetanized muscles is usually simulated using the classical Huxley-Simmons (HS) model. It predicts negative effective elastic stiffness in the state of isometric contractions (stall conditions), which can potentially trigger spatial inhomogeneity at the scale of the whole muscle fiber. Such instability has not been observed. Here we argue that the passive stabilization of the homogeneous state in real muscles may be due to the steric short-range interaction between individual myosin heads, which competes with the long-range elastic interaction induced by semi-rigid myosin backbones. We construct a phase diagram for the HS-type model accounting for such competing interactions and show that the resulting mechanical response in stall conditions is strongly influenced by a tricritical point. In addition to the coherent pre- and post-power stroke configurations anticipated by the original HS theory, the augmented model predicts the stability of configurations with pre- and post-power stroke cross-bridges finely mixed. In this new "phase," the overall stiffness of a half-sarcomere is positive, which suggests that it may be adequately representing the physiological state of isometric contractions.

INTRODUCTION

An isometrically constrained skeletal muscle reaches the stall conditions when it is fully tetanized. This physiological regime is known as the state of isometric contractions. Passive mechanical response in this state is usually tested through abrupt mechanical perturbations [1–4]. In particular, such tests provided a detailed picture of the power stroke machinery responsible for the fast force recovery, a transient passive response that does not involve the detachment of myosin heads [5].

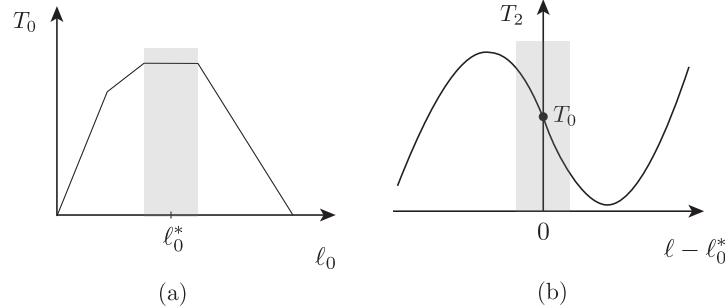


Figure 1. (a) Isometric tetanus: actively generated force T_0 as a function of the reference length ℓ_0 . (b) Quasi-equilibrium states T_2 reached from the stall state T_0 by fast shortenings or stretches. Highlighted are the main physiological regimes.

In experiments, the muscle is held at the extremities (length clamp or hard device loading) in an appropriate physiological solution while being electro-stimulated. Under these conditions, it actively generates a stall force (isometric tension) T_0 , which depends on sarcomere length ℓ_0 , see the schematic picture in Fig. 1(a). The muscle is then shortened (or stretched) by a fixed amount, and the generated tension is measured. For instance, if a (negative) displacement $\delta\ell = \ell - \ell_0^*$ is applied to a muscle, isometrically contracting at length ℓ_0^* , the tension first drops to the level $T_1 < T_0$, but then recovers in a few millisecond time scale to the higher level T_2 , see the schematic picture in Fig. 1(b). A more detailed picture of the actual experiment together with the available experimental measurements are shown in Fig. 2 (a,b).

While the initial response T_1 is attributed to passive elasticity of myosin heads (cross-bridges) [1, 6], the recovered tension T_2 results from a conformational transition inside actin-bound myosin heads. During this transition, some of the cross-bridges switch (or fold) from pre to post power stroke state [5, 7]. Such folding is believed to be a purely mechanical process as it does not involve the un-binding of myosin heads from actin filaments[8].

Since the homogeneous state of isometric contractions is a homeostatic (stable) equilibrium, the corresponding global elastic stiffness $dT_2/d\ell$ should be positive, and this is indeed what was observed in the pioneering experiments

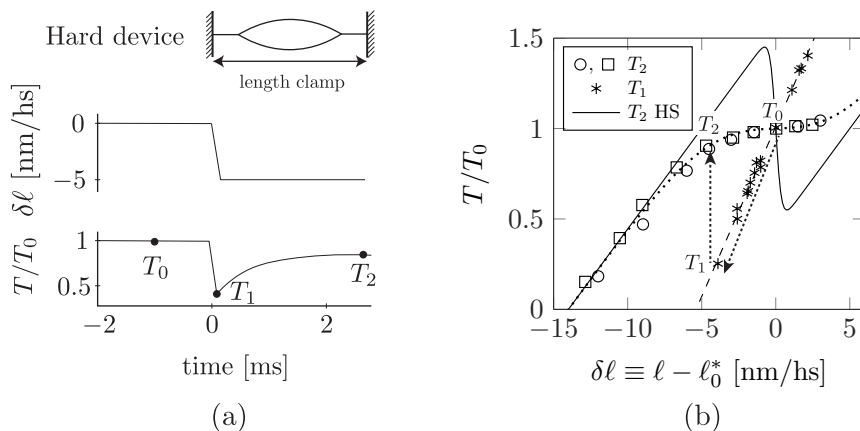


Figure 2. (a) Fast transients in mechanical experiments on single muscle fibers. In response to the length step $\delta\ell$, the tension first drops from T_0 to T_1 and then recovers a fraction of the initial tension, reaching the level T_2 . (b) The recovered tension T_2 as a function of the imposed stretch $\delta\ell$. Solid curve shows the predictions of the HS model with realistic parameters: $a = 10\text{nm}$, $\kappa_0 = 2\text{pN/nm}$, $T = 277.15\text{K}$, $v_0 = 24.4\text{pN}$ [4, 9]. Data extracted from [10–12]

of Huxley and Simmons (HS) [1], see Fig. 2(b). They proposed a theoretical explanation for their measurements, arguing that the elementary force-generating units contain at least two structural elements connected in series. The first one is an elastic spring responsible for generating the tension T_1 , which can be modeled as Hookean. The second is a bi-stable power stroke element that can be either in pre- or in post-power stroke position. HS modeled it as a hard-spin variable representing the angular position of the myosin head with respect to actin.

To ensure a collective response, individual myosin heads interact non-locally through actin and myosin filaments bundled by elastic disks. They also interact directly (sterically) or through the environmental substances. A mean-field long-range interaction through an almost rigid backbone was first introduced by HS[1]. They studied a thermomechanical behavior of such (paramagnetic) force generating units (half-sarcomeres) in a chemo-mechanical setting with pre- and post-power stroke conformations presented as chemical states. HS used the Kramers approximation, but their model was recently generalized to account for the full-scale Langevin dynamics [13–16].

The hard spin HS model can reproduce the experimentally measured tension T_2 but only if the stiffness of myosin heads is underestimated. If the correct value ($2.7 \pm 0.9 \text{ pN}\cdot\text{nm}^{-1}$, [6, 17, 18]) is used, the HS model leads to the controversial prediction that the free energy of a half-sarcomere is a non-convex function of strain, which means, in particular, that the effective stiffness in the physiological stall force regime is negative [19, 20], see Fig. 1(b) and Fig. 2(b). Behind the non-convexity of the free energy is the highly coherent mechanical response of interacting cross-bridges, which essentially precludes the mixing of pre- and post-power stroke configurations: given the value of the environmental temperature, the strong mean-field interaction ensures that all are either in the pre-power stroke or all in the post-power stroke state.

The non-positive-definiteness of the tangential elasticity in the constitutive model suggests the possibility of mechanical instability of the homogeneous (affine) response for the corresponding 'muscle material'. In particular, spatial inhomogeneity should be present in muscle fibers modeled as series connections of half-sarcomeres [19, 21]. Individual half-sarcomeres will be then either entirely in pre- or post-power stroke configurations, which can be interpreted as a coexistence of pure phases. Even though this would lead to a realistically flat T_2 curve in the regime of isometric contractions, the corresponding fiber will be structurally highly inhomogeneous [19, 21, 22]. The fact that such inhomogeneity has not been observed in experiments stimulated theoretical efforts to account for physical factors ensuring the mixing of the pre- and post-power stroke configurations at the scale of individual half-sarcomeres. Different mechanisms facilitating such mixing have been proposed in the literature.

Efforts to suppress the instability of an affine response have started already with A. Huxley himself, who suggested that the mixing can be explained by the inherent randomness encapsulated in actomyosin machinery [23]. Indeed, experiments involving electron microscopy [24, 25] and X-ray diffraction [5, 26], reveal a much more complex geometrical structure of the actomyosin complex than in the original HS model. For instance, myosin binds to actin only in specific target zones, which are not commensurate with the spacing of myosin heads. As a result, different binding sites are reached at different angles [25, 27]. The implied quenched disorder will compromise the coherent response, and the implications of this general idea have been recently thoroughly tested [28]. In particular, it was shown that

having a structural disorder in the positions of myosin molecules relative to attachment sites can effectively convexify the elastic response and flatten the T_2 curve. The most striking result was that a realistic disorder places the muscle system close to a critical point [20, 28].

Local mixing of the pre- and post-power stroke configurations can also be facilitated by an active process. As shown in [29], the presence of correlated external excitations can generate positive rigidity in the system, which has otherwise negative rigidity and is then unstable. In particular, such positive active rigidity can overcome the negative passive rigidity in the HS model, making the affine response stable. The coherency of the mean-field-dominated configurations will then be broken because each element will be forced to stay away from a single energy well. Note that the ensuing mixing will be active and different from the passive 'melting' taking over at high temperatures. The only problem with the active stabilization is that it requires additional incessant ATP consumption.

It is then natural to explore the possibility of a passive stabilization of affine response. With this aim in view, we assume in this paper that the highly coherent mechanical response of muscle half-sarcomeres is compromised by the destabilizing steric short-range interaction between individual myosin heads, which competes with the stabilizing long-range interaction imposed by the semi-rigid myosin filaments. To support this hypothesis, we now recall some experimental observations.

It is commonly accepted that cross-bridges in isometrically contracting myofibrils move through power stroke asynchronously and assume, at any moment of time and in any given location, two distinct conformations [30–33]. In particular, it is known that at the steady-state plateau of isometric tetanus, see Fig. 1(a), the individual myosin motors are in different conformations, which is sometimes interpreted as the state of disorder. Apparently, the cross-bridges get synchronized spatially and temporarily only in response to very rapid stretches or slacks and, in this sense, the fast force recovery is sometimes interpreted as a disorder-to-order transition [34].

However, these interpretations remain qualitative since the usual mechanical and structural measurements at the single half-sarcomere level deal predominantly with populations of myosin motors. This makes it difficult to follow the change in conformation of individual cross-bridges and quantify the process of stress-induced synchronization [6]. Still, specially designed X-ray experiments can provide at least some access to the spatial distribution of the myosin motors. For instance, one can use the width of the third-order myosin based meridional reflection (M3 reflection) because it can be related to the number of myosin motors in the pre-power stroke state. Similarly, the splitting of the M3 reflection can be linked to the distance between the two arrays of myosin motors in pre- and post- power stroke states [35]. With these and other experimental approaches, it has been confirmed that while at loads closer to stall conditions myosin motors are broadly distributed, at lower loads they proceed through the stroke almost collectively [36, 37].

Such measurements, however, still provide information only about the homogenized state. If, for instance, the averaged observed state in the quenched configuration is between pre- and post-power stroke, they do not reveal the actual geometrical pattern behind them. On a theoretical side, the assumption that individual myosin heads interact only through the thick filament, modeled as a rigid backbone, does not allow one to make any conclusions about the spatial organization of pre- and post-power stroke cross-bridges inside a single half-sarcomere. To identify the implied patterns, at least in silico, it is necessary to go beyond the class of mean-field models and account explicitly for short-range interactions involving the neighboring cross-bridges.

In this regard, it is appropriate to mention that since the power stroke represents the sliding of ~ 10 nm [38] while the distance between protrusions, representing myosin heads, is ~ 14.5 nm [39], the size of the working stroke is comparable to the distance between neighboring myosin heads. Therefore, whether a particular myosin head is in pre- or post-power stroke position will influence its neighbors' state, hence the local patterning may be guided by such steric interaction. Moreover, such short-range interaction may involve first and second heads, and adjacent tropomyosin-troponin regulatory units. It may also depend on the coupling between regulatory units and cross-bridges [40]. Yet another important factor is that the rigidities of the thick and thin filaments are comparable to those of the cross-bridges. The account of filament extensibility will make the relative displacements of the neighboring cross-bridges generically non-uniform [41, 42]. As a result, the local configuration of an attached myosin head will be affected elastically by the state of the neighboring heads. In particular, the account for elastic effects can make the coherent configurations with larger averaged spacing energetically less preferable than the 'closed packed' interdigitated configurations with pre- and post-power stroke cross-bridges periodically patterned.

To rationalize such possibilities, in this paper, we complement the mean-field interaction of HS, favoring uniformity of micro-configurations, with the short-range steric interactions favoring the mixing of pre- and post-power stroke states. More specifically, we make the antiferromagnetic interaction between neighboring spins compete with the long-range paramagnetic interaction of HS. The ensuing 1D hard-spin model of a muscle half-sarcomere can be viewed as a version of the corresponding Ising model where various short- and long-range interactions are allowed to compete. Such competition can generate a rich repertoire of thermodynamic behaviors [43–47] and the goal of

this paper is to explore different alternatives in the context of muscle mechanics. An additional complication is that the HS mean-field interaction makes the ensuing systems non-additive, which leads to ensemble inequivalence. In particular, the isometric and the isotonic mechanical responses will be necessarily different and would have to be treated separately [47–50].

Our study shows that if the antiferromagnetic short-range interactions are sufficiently strong, the HS-type coherent single-state isometric response of skeletal muscle is destabilized. Instead, we obtain a non-HS response with cross-bridges in pre- and post-power stroke configurations finely mixed. Moreover, we show that in such regimes the cross-bridges necessary form a regular interdigitated pattern. The macroscopically homogeneous response of a muscle fiber is then recovered at the expense of the configurations of individual half-sarcomeres becoming maximally inhomogeneous. The presence of short-range interaction is then responsible for generating a new energy well, which we associate with the physiological state of isometric contractions. The fact that the macroscopically homogeneous response is stabilized passively makes our approach fundamentally different from the one involving active stabilization [29]. We also note that the energy wells, different from the ones describing pre and post power stroke states, are introduced routinely in the phenomenological chemo-mechanical models to ensure that the $T_2(\delta\ell)$ curve is sufficiently flat around the stall state [51, 52]. Such three-state systems would be represented by the Potts model, whose main prediction is the existence of a tri-critical point separating the line of first- and second-order transitions [53, 54]. In our minimal two-well model, the third ‘phase’ is emerging naturally after averaging and the tri-critical point arises without any additional phenomenological assumptions.

Our main result is an equilibrium phase diagram. In addition to the ‘coherent’ bi-stable phase predicted by the original HS theory and the ‘melted’ phase appearing at high temperatures, the obtained phase diagram shows the existence of a domain with configurations of the antiferromagnetic type containing both pre- and post-power stroke cross-bridges. Having such configurations is physiologically beneficial for the system, which could then anticipate the necessity of either ultrafast contraction (global switching to post-power stroke state) or ultrafast stretching (global switching to pre-power stroke state). The whole phase diagram is effectively controlled by a tricritical point, and we argue that a living system may benefit from being posed near such a singular point.

The paper is organized as follows. In Section 2, we introduce the model and show how it can be analyzed at zero temperature. In Section 3, we consider finite temperatures and construct the main phase diagram for the system in a hard device. In Section 4, we study the system in a soft device and illustrate the ensemble non-equivalence. We then specify in Section 5 the order parameters and study spatial correlations. The case study of two half-sarcomeres in series is presented in Section 6. Finally, in Section 7 we summarize our results.

THE MODEL

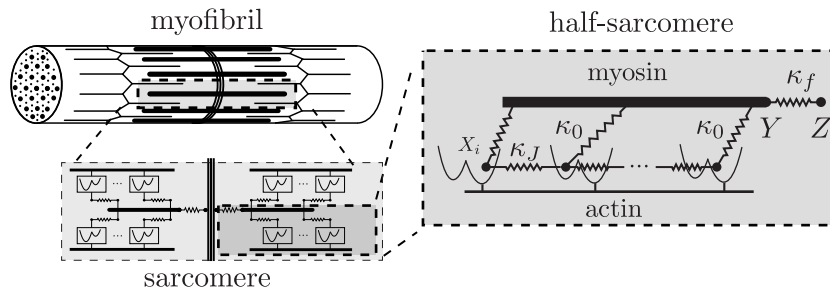


Figure 3. Half-sarcomere modelled as a parallel cluster of Huxley-Simmons units with additional short-range interactions between the neighboring cross-bridges.

Following HS, we model a half-sarcomere as a collection of N interacting cross-bridges, but we supplement the mean-field interaction introduced of HS by a competing short-range interaction.

The energy of non-interacting cross-bridges can be written as

$$\sum_i^N V(X_i),$$

where $i = 1, \dots, N$ and $V(X_i)$ is a double-well energy of a single cross-bridge, see Fig. 3. We assume for analytical

simplicity that the two conformational positions of the myosin head are represented by the hard spin variable X_i so that in the pre-power stroke state $X_i = 0$, and in the post-power stroke state $X_i = -a$, where a is the amount by which the myosin head pulls the actin during the power stroke. We set that $V(X_i) = (a + X_i)V_0$ which shows that the pre-power stroke conformation has higher energy than the and post-power stroke conformation with the energy bias equal to V_0 , see Fig. 4. Despite the overall passive nature of the HS model, this bias V_0 has an active origin because it is ultimately responsible for the constant tension T_0 in the state of isometric contractions.

In the HS model each cross-bridge is connected to a common rigid backbone through an elastic spring κ_0 placed in series with a bi-stable unit. The backbone is characterized by a single variable Y and the corresponding interaction energy is of mean-field type

$$\sum_i^N \frac{\kappa_0}{2} (Y - X_i)^2,$$

where $\kappa_0 > 0$ is a parameter stabilizing homogeneous distribution of cross-bridge configurations.

In addition to this interaction we assume that each element also interacts harmonically with its nearest neighbors through the energy term

$$\sum_i^N \frac{\kappa_J}{2} (X_{i+1} - X_i)^2,$$

where κ_J is the corresponding via a linear stiffness. This short-range interaction is perceived to have a steric origin and may originate from the presence of additional myosin heads. To have a destabilizing effect on the homogeneous distribution of cross-bridges favored by the mean-field interaction, the parameter κ_J should be able to take negative values.

Finally, we assume that the whole half-sarcomere is loaded through an elastic spring with stiffness $\kappa_f > 0$, representing the combined elasticities of actin and myosin filaments. When the system is loaded in a hard device, an imposed displacement Z is applied to the external spring giving the contribution to the energy

$$\sum_i^N \frac{\kappa_f}{2N} (Z - Y)^2.$$

The whole mechanical system representing a single half-sarcomere is illustrated as the largest zoom in Fig. 3.

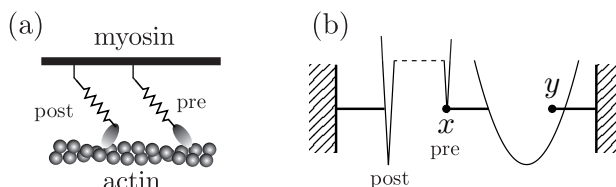


Figure 4. (a) Schematics showing two neighboring cross-bridges in different conformational states, (b) Huxley-Simmons (HS) model of a single cross-bridge. The two conformational states of the myosin head are represented by the spin variable x while the lump elasticity of the whole cross-bridge is represented by the parabolic potential acting on the continuous variable y .

To non-dimensionalize the problem we define the reference length a , and normalize the spatial variables accordingly: $x_i = X_i/a$, $y = Y/a$ and $z = Z/a$. Note that now the variable x_i takes values 0 and -1 for the pre- and post-power stroke, respectively. Using $\kappa_0 a^2$ as the scale of the energy we obtain in dimensionless variables

$$E(\mathbf{x}, y, z) = \sum_i^N (1 + x_i)v_0 + \frac{1}{2}(y - x_i)^2 + \frac{\lambda_J}{2}(x_{i+1} - x_i)^2 + \frac{\lambda_f}{2}(z - y)^2. \quad (1)$$

We consider periodic boundary conditions: $x_{N+1} = x_1$, however, in the thermodynamic limit $N \rightarrow \infty$, the choice of this type of boundary conditions becomes irrelevant [54, 55]. The ensuing problem contains two dimensionless parameters $\lambda_J = \kappa_J/\kappa_0$ and $\lambda_f = \kappa_f/(N\kappa_0)$.

To reveal the main effect it is sufficient to analyze the system at zero temperature. To obtain the ground state, we

first eliminate y using the condition $\partial E/\partial y = 0$, which is equivalent to

$$y = \frac{\lambda_f z}{1 + \lambda_f} + \frac{1}{N(1 + \lambda_f)} \sum_i x_i. \quad (2)$$

The relaxed energy is of Ising form with both mean-field and short-range interactions:

$$E(x_i, z) = -\frac{J}{2N} \sum_{i,j} x_i x_j - \lambda_J \sum_i x_i x_{i+1} - h(z) \sum_i x_i + c(z). \quad (3)$$

where $1/J = 1 + \lambda_f$ and

$$h(z) = \frac{\lambda_f z}{1 + \lambda_f} - v_0 + \lambda_J + \frac{1}{2}, \quad c(z) = \frac{N\lambda_f z^2}{2(1 + \lambda_f)} + Nv_0.$$

Since this energy is quadratic in z at a given x_i , the minimization over x_i reduces to the choice among a finite number of parabolas.

Depending on the values of λ_J and λ_f , the global minima correspond to either pure phases, with all cross-bridges synchronized in the same conformational state (pre- or post-power stroke), or to a mixed phase with lattice scale oscillations between the two conformational states. At a not too negative value of λ_J , the energy minimizing phase is ferromagnetic with pre- or post-power stroke state dominating depending on whether the system is stretched or compressed. At sufficiently negative λ_J , when destabilizing short-range interactions are strong, the unstressed system can also be in an antiferromagnetic state when neighboring cross-bridges are in opposite conformational states.

The phase diagram, revealing the structure of the ground state in the unstressed state, is presented in Fig. 5(a). The boundary separates the antiferromagnetic (mixed) and ferromagnetic (pure) ground states. We assumed here, for simplicity, that the unstressed state describes the stall condition and also arbitrarily set that in this state, the distribution of pre- and post-power strokes cross-bridges is 50-50 [56]. We therefore have the stall state at $z = z_0 = (1 + 1/\lambda_f)v_0 - 1/2$ where post- and pre-power stroke conformations have the same energy. Note that at $z = z_0$ the energies of pure and mixed configurations become equal if $1/\lambda_J = -4(1 + \lambda_f)$. At

$$\lambda_J < -\frac{1}{4(1 + \lambda_f)}$$

the equilibrium configuration in stall conditions is mixed while it is coherent (all cross-bridges are either pre- or post-power stroke) otherwise. In the limiting case $\lambda_f \rightarrow \infty$, when cross-bridges interact only at short-range, the transition occurs at $\lambda_J = 0$. In the other limiting case $\lambda_f \rightarrow 0$, the crossover between ferromagnetic and antiferromagnetic phases takes place at $\lambda_J = -1/4$.

We now compare the energies of different spatial distributions x_i at $z = z_0$. In the FM phase, any of the mixed configurations will have higher energy than one of the pure configurations $E_{mixed}(z = z_0) > E_{pure}(z = z_0)$, while in the AFM phase $E_{mixed}(z = z_0) < E_{pure}(z = z_0)$. Here E_{pure} can be taken as the energy of a configuration with either all pre- or all post-power stroke cross-bridges because at $z = z_0$ they are equal.

In Fig. 5(b)(ii, iv) we show the energies of local and global minimizers $E(z)$ corresponding to mixed (alternating pre- and post-power stroke states) and pure (fully synchronized) configurations that are parameterized by z . The corresponding branches of tension-elongation curves $t = dE/dz$ are shown in Fig. 5(b)(i,iii).

It is interesting that in the tension curves 5(b)(i, iii), different metastable branches are uniquely characterized by the total amount of spins in either pre- or post-power stroke, which means that from developed tension alone we cannot distinguish spatial organization. To this end, we need to turn to the energy function. The reason comes directly from the energy (3) where all z related terms are in h and c , which means that both short- and long-range terms (J and λ_J , respectively) are z insensitive, and only the average 'magnetization' $\sum_i x_i$ interacts with the loading device. However, ultimately the choice of the most stable branch is dictated by the energy.

We also note that in the ferromagnetic phase, the macroscopic stiffness in the stall state is equal to minus infinity. In the antiferromagnetic phase, the transition between the two pure states is smoothed, but the stiffness in the stall state remains to be equal to minus infinity. This means that the formal 'stabilization' of this state is impossible at zero temperature.

To summarize, the analysis of the zero temperature system shows that due to the mean-field nature of ferromagnetic interactions, the preferred behavior is coherent with fully relaxed energy remaining non-convex and the corresponding stiffness taking negative values. Adding sufficiently strong short-range antiferromagnetic interactions partially

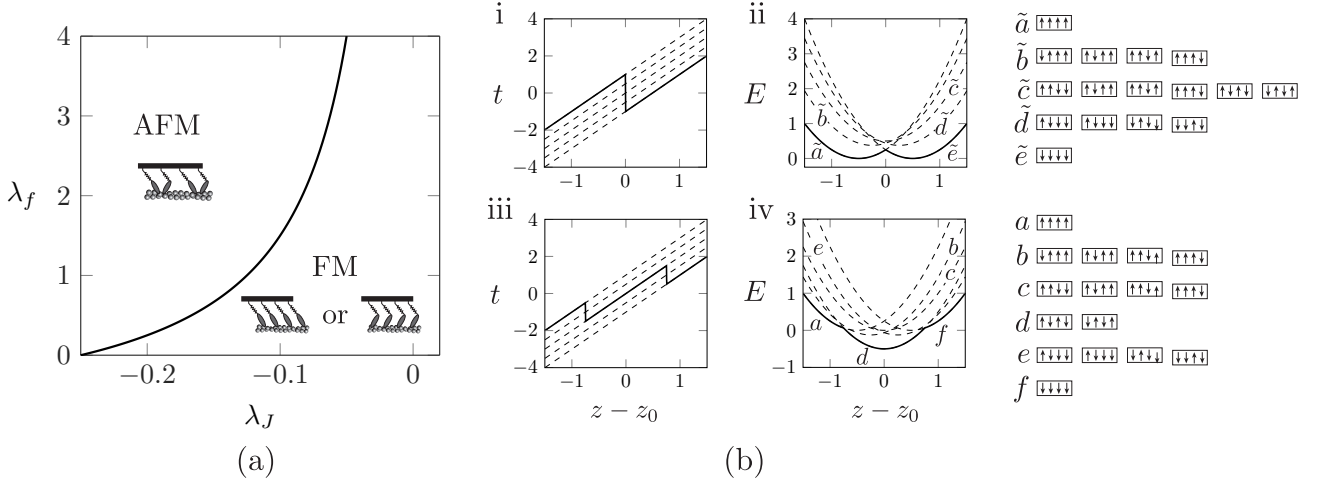


Figure 5. (a) Zero temperature phase diagram for a half sarcomere in the stall state $z = z_0$. (b) Energy and tension of a system of $N = 4$ cross-bridges. The thick solid line represents the global minimum of the energy (ground state), while the dashed line represents the local energy minima (metastable states). In i–ii we illustrate the ferromagnetic (FM) part of the phase diagram (corresponding to $\lambda_f = 1$, $\lambda_J = 0$); and in iii–iv, the antiferromagnetic (AFM) part (corresponding to $\lambda_f = 1$, $\lambda_J = -0.5$). In (b) each metastable branch is associated with a particular micro-configuration, which is illustrated in the right column. The "up/down" arrows represent pre/post power stroke states.

convexifies the relaxed energy; however, negative stiffness persists.

EQUILIBRIUM RESPONSE

To study the equilibrium response of the system at finite temperature θ , we need to compute its free energy. The partition function in the *hard device* ensemble (controlled displacement) is,

$$\mathcal{Z}(\beta, z) = \int dy \sum_{\{x\}} e^{-\beta E(x_i, y, z)},$$

where the summation is over $x_i = \{0, -1\}$ for all x_i ; we also use the standard notation $\beta = \kappa_0 a^2 / k_B \theta$, where k_B is the Boltzmann constant. Since $\sum_i x_i^2 = -\sum_i x_i$, we can write

$$\mathcal{Z}(\beta, z) = \int dy e^{-\beta N \varphi(y, z)} \mathcal{Z}_0(\beta, y), \quad (4)$$

where $\varphi(y, z) = \frac{\lambda_f}{2} (z - y)^2 + v_0 + \frac{y^2}{2}$ and the function $\mathcal{Z}_0(\beta, y)$ is the partition function for an Ising ring [55]:

$$\mathcal{Z}_0(\beta, y) = \sum_{\{x\}} \exp \left[\beta J \sum_i x_i x_{i+1} + \beta H \sum_i x_i \right], \quad (5)$$

where, $J = \lambda_J$ and $H(y) = \lambda_J + y + 1/2 - v_0$. The equilibrium behavior of this system without short-range interactions ($\lambda_J = 0$) was studied in [15].

To compute $\mathcal{Z}_0(\beta, y)$ we can use the transfer matrix method [47, 57]. The idea is to represent this partition function as a product of equal matrices [54, 55]. Consider the matrix

$$\mathbf{T} = \begin{pmatrix} 1 & e^{-\frac{\beta H}{2}} \\ e^{-\frac{\beta H}{2}} & e^{\beta(J-H)} \end{pmatrix}. \quad (6)$$

Then, $\mathcal{Z}_0 = \text{Tr}(\mathbf{T}^N)$, and since \mathbf{T} is real and symmetric, it can be diagonalized with the eigenvalues

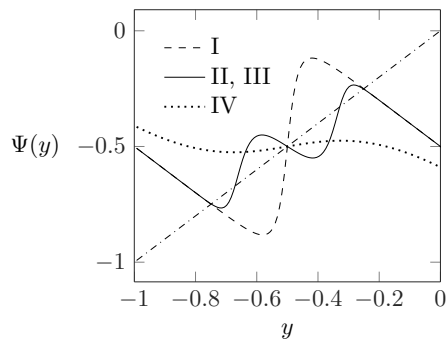


Figure 6. Different solutions of the self-consistency condition (10) correspond to interactions of different curves with an inclined straight line. In phase I, there are three solutions (two energy minima, two symmetric ground states), in phases II and III, there are five solutions (three energy minima with either one or two (symmetric) ground states), and in phase IV, the solution is unique (single energy minimum which is also the ground state).

$$\lambda_{1,2} = e^{-h} \left[\cosh h \pm \sqrt{\sinh^2 h + e^{-\beta J}} \right], \quad (7)$$

where $h = \frac{\beta}{2}(H - J)$. Using the invariance of the trace we obtain $\mathcal{Z}_0 = \lambda_1^N + \lambda_2^N$. If we now assume that $\lambda_1 > \lambda_2$, and take the thermodynamic limit $N \rightarrow \infty$, we obtain $\mathcal{Z}_0 \approx \lambda_1^N [1 + \mathcal{O}(e^{-\alpha N})]$, where $\alpha \equiv \log(\lambda_1/\lambda_2)$ is a positive constant. Using the Laplace method we finally obtain,

$$\mathcal{Z}(\beta, z) \sim \min_y \left\{ e^{-\beta\varphi(y,z)} \lambda_1(y) \right\}. \quad (8)$$

The free energy density is $\mathcal{F}(\beta, z) = -\frac{1}{N\beta} \log \mathcal{Z}(\beta, z)$. In the thermodynamic limit we can write

$$\mathcal{F}(\beta, z, y) = \frac{\lambda_f}{2}(z - y)^2 + v_0 + \frac{y^2}{2} + \frac{g(y)}{\beta} - \frac{1}{\beta} \log \left[\cosh g(y) + \sqrt{e^{-\beta\lambda_J} + \sinh^2 g(y)} \right]. \quad (9)$$

where $g(y) = \frac{\beta}{2}(y + 1/2 - v_0)$. By solving a transcendental equation $\partial\mathcal{F}(\beta, z, y)/\partial y = 0$ we obtain the self-consistency relation $y_* = \Psi(\beta, z, y_*)$ illustrated in Fig. 6 with the function $\Psi(y_*)$ known explicitly

$$\Psi(\beta, z, y) = \lambda_f(z - y) - \frac{1}{2} + \frac{1}{2} \frac{\sqrt{e^{-\beta\lambda_J} + \sinh^2 g(y)}}{e^{-\beta\lambda_J} \operatorname{csch} g(y) + \sinh g(y)}. \quad (10)$$

As we show in Fig. 6, the equation (10) may have more than one solution, which reflects the non-convexity of the partial free energy $\mathcal{F}(\beta, z, y)$. The parametric dependence of this energy is illustrated in Fig. 7 for the stall state with $z = z_0$. Four different phases can be identified on the plane $(\lambda_J, 1/\beta)$. The zero temperature phase diagram shown in Fig. 5(a) corresponds to the first-order transition boundary separating phases II and III and is represented in Fig. 7 by its section at $\lambda_f = 1$.

In the domain with low temperature and dominating mean-field interactions, we observe Phase I. In this Phase, two pure states coexist, but at any instant of time, all cross-bridges are either in pre- or post-power stroke conformations. In other words, in stall conditions, the system in Phase I randomly switches between these two states. Each of these transitions takes place coherently, with all cross-bridges changing their state cooperatively. In the high-temperature domain and still dominating mean-field interactions, we observe phase IV, where all cross-bridges switch randomly and independently between pre- or post-power stroke conformations. Phase IV is separated from Phase I by a second-order phase transition, analogous to the usual order-disorder transition in magnetics.

At low temperatures and strong short-range antiferromagnetic interactions, we observe the appearance of Phases II and III, where in addition to pure states, there is also a mixed state where neighboring cross-bridges have different conformations. In Phase II, the mixed state is metastable, and the equilibrium states are the pure ones, while in Phase III, the equilibrium state is the mixed one. Phases II and III are separated by the line of first-order phase transition, which meets the second-order phase transitions line separating Phases I and III at a tricritical point.

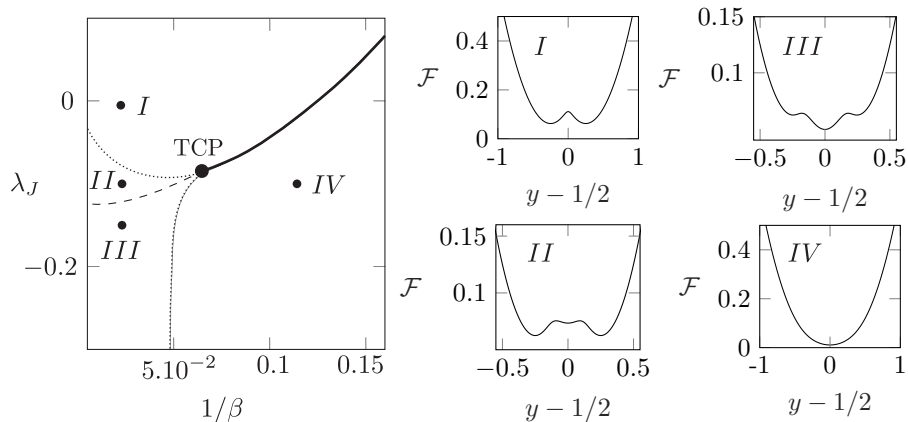


Figure 7. (a) Phase diagram for the system in the hard device with $z = z_0$. Parameters: $\lambda_f = 1$, $v_0 = 0$. The transition between phases I and IV is continuous (bold solid line) down to the tricritical point TCP, where it becomes first-order (dashed line). The dotted lines are spinodal boundaries. The different phases are illustrated in the right column, where we show the dependence of the partial free energy \mathcal{F} on the internal variable y .

To summarize, when the short-range interactions are sufficiently strong and the temperature is sufficiently low, we observe a new feature in the system's behavior: an antiferromagnetic state becomes stable in the stall regime $z = z_0$ (our Phase III). In other low-temperature Phases I and II, the stall state must necessarily involve random coherent conformational changes involving all cross-bridges simultaneously. At high temperatures, the paramagnetic phase dominates where all cross-bridges fluctuate randomly and independently over the whole energy landscape with neither pre- or post-power stroke stated clearly discernible. We have seen that by increasing λ_J in the positive direction, we effectively decrease the temperature by favoring cooperativity and effectively destabilizing the homogeneous state at $z = z_0$. Instead, by increasing λ_J in the negative direction, we disfavor coherent fluctuations between pure states at $z = z_0$ and stabilize instead nonfluctuating macroscopically homogeneous state, which we later show to be microscopically a fine lattice-scale mixture of pre- and post-power stroke conformations.

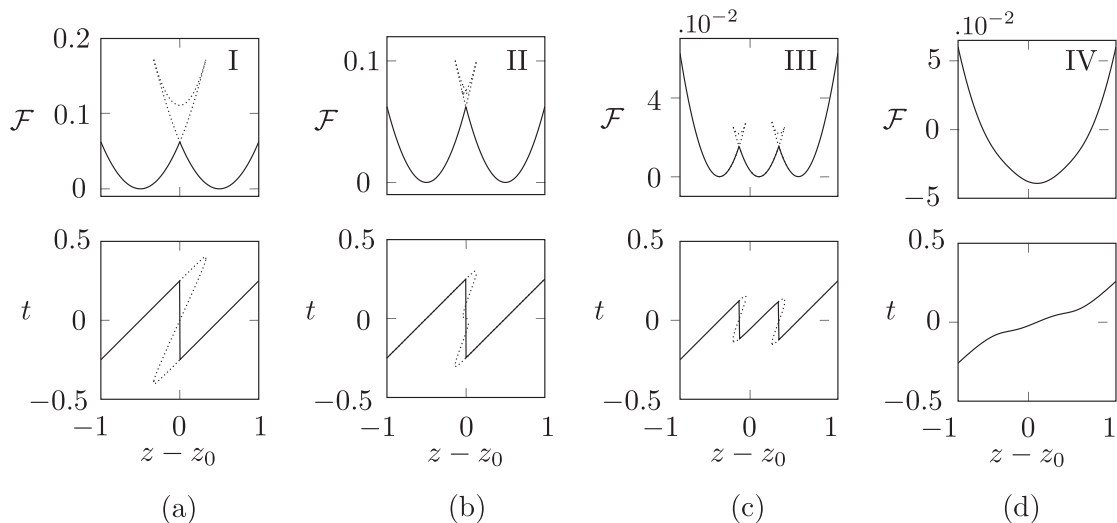


Figure 8. The equilibrium free (Helmholtz) energy-strain relation in the hard device and the corresponding tension-strain relation. (a) Phase I: $\lambda_J = 0$, $\beta = 50$; (b) Phase II: $\lambda_J = -0.1$, $\beta = 50$; (c) Phase III: $\lambda_J = -0.25$, $\beta = 50$; and (d) Phase IV: $\lambda_J = -0.25$, $\beta = 8$. Other parameters: $\lambda_f = 1$ and $v_0 = 0$. Solid curves correspond to ground states, dotted lines show some other stable and unstable equilibria.

We now turn to the parametric behavior of the equilibrium free energy $\mathcal{F}(z) = \mathcal{F}(z, y_*(z))$. Knowing this energy one can also compute the equilibrium tension $t(z) = d\mathcal{F}(z)/dz = d\mathcal{F}(z, y_*(z))/dz = \partial\mathcal{F}(z, y_*(z))/\partial z = \lambda_f(z - y_*(z))$,

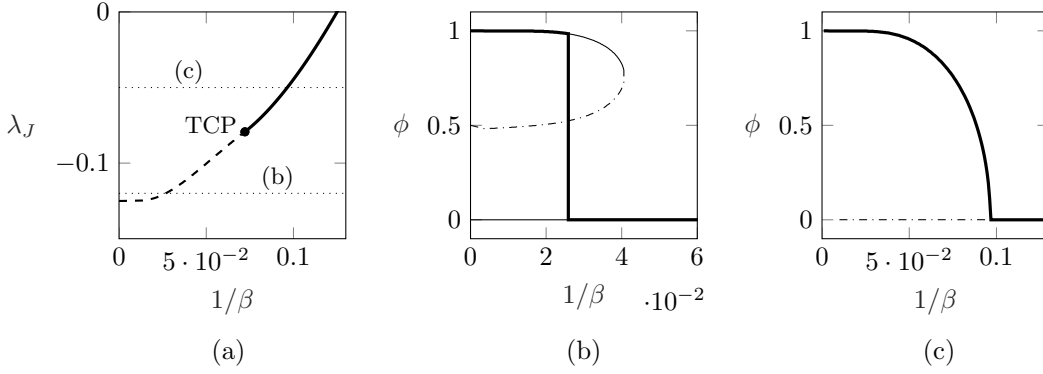


Figure 9. (a) Phase diagram in the hard device with $z = z_0$. Second-order transitions are shown by a solid bold line, first-order phase transitions by a dashed bold line. The dotted lines indicate the locations of the two representative sections shown in (b) and (c). (b) First-order phase transition, $\lambda_J = -0.12$. Thin solid lines correspond to metastable states, dash-dotted line – to unstable states; (c) Second-order phase transition, $\lambda_J = -0.05$. The dash-dotted line corresponds to unstable states.

where we temporarily omitted dependence on β . The behavior of the functions $\mathcal{F}(z)$ and $t(z)$ in different phases is illustrated in Fig. 8. Note that in (a) and (b) (Phases I and II), the free energy is non-convex at $z = z_0$, and the corresponding stiffness is negative. Instead, in (c) and (d) (Phases III and IV), the stall state is associated with the point of convexity of the equilibrium energy, and the corresponding stiffness is positive. However, if in Phase IV we deal with entropic stabilization at the expense of an identifiable conformational state, in Phase III, we encounter macroscopic homogeneity with the perfect antiferromagnetic order where each cross-bridge maintains its conformation with one half of them being in pre- and another half in post-power stroke state.

To obtain an analytical expression for the line of critical points (and ultimately for the tricritical point where it ends) on the phase diagram shown in Fig. 7, we can build around it a polynomial, Landau type expansion [55, 58].

To define an order parameter we recall that, according to (2), the average value of the microscopic spin variable $\langle x \rangle = N^{-1} \sum_i x_i$ is related to the macroscopic variable y through the relation $\langle x \rangle = (\lambda_f + 1)y - \lambda_f z$. Since $E(x_i = 0, z_0) = E(x_i = -1, z_0)$, in stall conditions $z = z_0$ the fraction of post-power stroke elements should be equal to the fraction of pre-power stroke elements, which suggests that $\langle x \rangle(\beta, z_0) = -1/2$. Then the natural order parameter is $\phi = 2\langle x \rangle + 1$, or equivalently, $\phi = 2(\lambda_f + 1)y - 2\lambda_f z + 1$. It now represents the fraction of elements in either conformation, meaning that with $\phi = 1$ all units are in the pre-power stroke, and with $\phi = -1$ in the post-power stroke configuration. Finally, $\phi = 0$ means that there are equal number of elements in both conformations.

The marginal free energy at $z = z_0$ can be now written in terms of ϕ

$$\mathcal{F}(\beta, \phi) = \frac{1}{2} \left(v_0 + \frac{1}{2} \right)^2 + \frac{v_0^2}{2\lambda_f} + \frac{\phi^2}{8(1 + \lambda_f)} - \frac{1}{\beta} \log \left[\cosh \frac{\beta\phi}{4(1 + \lambda_f)} + \sqrt{e^{-\beta\lambda_J} + \sinh^2 \frac{\beta\phi}{4(1 + \lambda_f)}} \right]. \quad (11)$$

The corresponding self-consistency relation expressed in terms of ϕ_* takes the form

$$\phi_* = \frac{\sinh \frac{\beta\phi_*}{4(1 + \lambda_f)}}{\sqrt{e^{-\beta\lambda_J} + \sinh^2 \frac{\beta\phi_*}{4(1 + \lambda_f)}}}. \quad (12)$$

In Fig. 9 (b) and (c) we show the behavior of the function $\phi_*(\beta)$ around the lines of first- and second-order phase transitions (critical points), respectively, shown in Fig. 9(a). Our goal now is to capture the line of second-order phase transitions separating Phases I and IV. To this end it is sufficient to perform the Taylor expansion of the free-energy

Eq. (11) around $\phi = 0$. We obtain the expression $\tilde{\mathcal{F}}(\beta, \phi) = a_0 + a_2\phi^2 + a_4\phi^4$ where,

$$a_0 = \frac{1}{2} \left(v_0 + \frac{1}{2} \right)^2 + \frac{v_0^2}{2\lambda_f} - \frac{\log \left(\sqrt{e^{-\beta\lambda_J}} + 1 \right)}{\beta}, \quad (13a)$$

$$a_2 = \frac{1}{32(1 + \lambda_f)} \left[4 - \frac{\beta}{(1 + \lambda_f)\sqrt{e^{-\beta\lambda_J}}} \right], a_4 = \frac{\beta^3 (3e^{\beta\lambda_J} - 1)}{6144(1 + \lambda_f)^4 \sqrt{e^{-\beta\lambda_J}}}. \quad (13b)$$

The approximate self-consistency relation $d\tilde{\mathcal{F}}/d\phi = 0$ gives either $\tilde{\phi} = 0$ or

$$\tilde{\phi} = \pm 4(1 + \lambda_f) \sqrt{\frac{6\beta - 24(\lambda_f + 1)\sqrt{e^{-\beta\lambda_J}}}{\beta^3 (3e^{\beta\lambda_J} - 1)}}. \quad (14)$$

The critical inverse temperature is implicitly given by relation $4(1 + \lambda_f)\sqrt{e^{-\beta_c\lambda_J}} = \beta_c$, which corresponds to $a_2 = 0$. In the limit $\lambda_J \rightarrow 0$ we obtain $\beta_c = 4(1 + \lambda_f)$.

To locate the tricritical point (TCP) where the second-order phase transition becomes the first-order phase transition, we need to use the sixth-order expansion in the order parameter $\tilde{\mathcal{F}}(\beta, \phi) = a_0 + a_2\phi^2 + a_4\phi^4 + a_6\phi^6$ where the additional coefficient is

$$a_6 = \frac{\beta^5 (30e^{\beta\lambda_J} - 45e^{2\beta\lambda_J} - 1)}{2949120\sqrt{e^{-\beta\lambda_J}}}. \quad (15)$$

The tricritical point can be linked to the vanishing of the second and fourth-order terms in the expansion. Therefore, we obtain two equations $\beta = 4(1 + \lambda_f)e^{-\beta\lambda_J/2}$ and $e^{-\beta\lambda_J/2} = \sqrt{3}$. Their solution can be found explicitly $\beta_{TCP} = 4(1 + \lambda_f)\sqrt{3}$ and $\lambda_{TCP} = -\log 3/4(1 + \lambda_f)\sqrt{3}$. Finally, the location of the line of first-order transitions (Maxwell line) can be obtained by solving the equation $\mathcal{F}(\beta, \phi = 0) = \mathcal{F}(\beta, \phi = \phi_*)$, where

$$\phi_* = \pm \sqrt{\frac{-a_4 + \sqrt{a_4^2 - 3a_2a_6}}{3a_6}}. \quad (16)$$

The obtained analytical relations allow one, for instance, to estimate the minimal level of antiferromagnetic short-range interactions, which is necessary to ensure the stabilization of the macroscopically homogeneous configuration of cross-bridges in the stall state.

In our previous work [20, 28] we argued that the peculiarity of muscles mechanical response in the state of isometric contractions can be linked to the presence in the HS type models of muscle contraction of a critical point located in roughly the same range of parameters. Here we see that the appearance of an additional parameter λ_J , which scales the non-HS, short-range interactions, turns such a critical point into a critical line that ends in a tricritical point. The additional degeneracy of the system around such TCP can lead to new physical effects that may be physiologically advantageous and deserve a special study.

ENSEMBLE INEQUIVALENCE

Due to the presence in this system of long-range interactions, the phase diagrams corresponding to the cases of hard (isometric) and soft (isotonic) loading conditions may differ [59].

Suppose our half-sarcomere is loaded isototonically (in a soft device) by an applied force with dimensionless value $t = \bar{T}/\kappa_0 a$. We may then neglect the external spring κ_f and write the corresponding total energy as

$$G(\mathbf{x}, y, t) = \sum_i^N (1 + x_i)v_0 + \frac{1}{2}(y - x_i)^2 + \frac{\lambda_J}{2}(x_{i+1} - x_i)^2 - ty. \quad (17)$$

The partition function takes the form

$$\mathcal{Z}(\beta, t) = \int dy \sum_{\{x\}} e^{-\beta G(\mathbf{x}, y, t)}.$$

The corresponding Gibbs free energy, $\mathcal{G}(\beta, t) = -(1/(N\beta) \log \mathcal{Z}(\beta, t))$ can be again computed semi-explicitly in the thermodynamic limit $N \rightarrow \infty$. Using the combination of a transfer matrix approach and a Laplace method, we obtain

$$\mathcal{G}(\beta, t) = -ty_* + v_0 + \frac{y_*^2}{2} + \frac{g(y_*)}{\beta} - \frac{1}{\beta} \log \left[\cosh g(y_*) + \sqrt{e^{-\beta\lambda_J} + \sinh^2 g(y_*)} \right], \quad (18)$$

where $g(y_*) = \frac{\beta}{2}(y_* + 1/2 - v_0)$, and y_* is the solution of a transcendental equation

$$y_* = t - \frac{1}{2} + \frac{e^{\beta\lambda_J} \sinh g(y_*) \sqrt{e^{-\beta\lambda_J} + \sinh^2 g(y_*)}}{2e^{\beta\lambda_J} \sinh^2 g(y_*) + 2}. \quad (19)$$

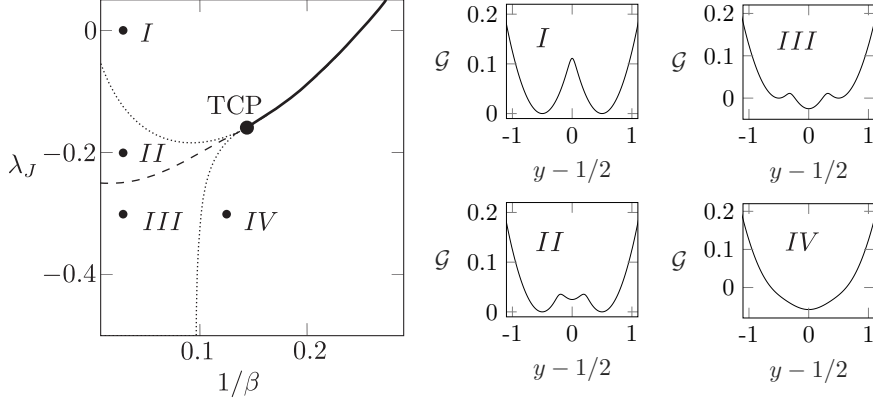


Figure 10. (a) Phase diagram for the system in the soft device at $t = 0$. Parameters: $\lambda_f = 1$, $v_0 = 0$. The transition between the phases I and IV is continuous (bold solid line) down to the tricritical point TCP, where it becomes first-order (dashed line). The dotted lines are spinodal boundaries. The different phases are illustrated in the right column where we show the dependence of the partial free energy \mathcal{G} on the internal variable y .

The parametric behavior of the marginal free energy $\mathcal{G}(\beta, y, t)$ in the stall conditions $t = 0$ is illustrated in Fig. 10. We again observe the same four major regimes, I, II, III, and IV, which have the same meaning as in the case of hard device ensemble. However, the location of the boundary between Phases and the position of the tricritical point is now different, see Fig. 10(a). In Phase III, we observe that the Phase minimizing Gibbs free energy is antiferromagnetic with pre and post power stroke conformations of cross-bridges finely interdigitated (see below). We also see that in this Phase, the macroscopically homogeneous configuration stabilizes the stall state corresponding to the minimum (rather than maximum) of the energy.

As in the hard device ensemble, the parameter λ_J plays the major role in the behavior of the system, which we illustrate by showing in Fig. 11 the equilibrium free energy and the force-elongation relation. One can see that in Phases I and II, the stall state is represented by the macroscopic mixture of two pure states with all cross-bridges occupying coherently either pre- or post-power stroke configuration. Instead, in Phases III and IV, the stall state is homogeneous, and cross-bridges in different conformations are microscopically mixed. The difference again is that in Phase IV each cross-bridge is fluctuating independently between two conformational states, while in Phase III, neighboring cross-bridges are always in different conformations that are fixed in time.

Similarly to the case of the hard device, we can analytically find the location of the line of critical points separating Phases I and IV and determine the position of the tricritical point, see Fig. 10(a). To define the order parameter in the soft device case, we observe that the equilibrium of the system with respect to the variable y implies, $y = t + N^{-1} \sum_i x_i$. It is then natural to define the order parameter again as $\phi = 2 \langle x \rangle + 1$, which in the soft device case gives, $\phi = 2y + 1 - t$.

We again assume, for simplicity, $v_0 = 0$ and focus on the stall state $t = 0$. We can then write the partial Gibbs free energy in the form

$$\mathcal{G}(\beta, \phi) = \frac{1}{8} + \frac{\phi^2}{8} - \frac{1}{\beta} \log \left[\cosh \frac{\beta\phi}{4} + \sqrt{e^{-\beta\lambda_J} + \sinh^2 \frac{\beta\phi}{4}} \right]. \quad (20)$$

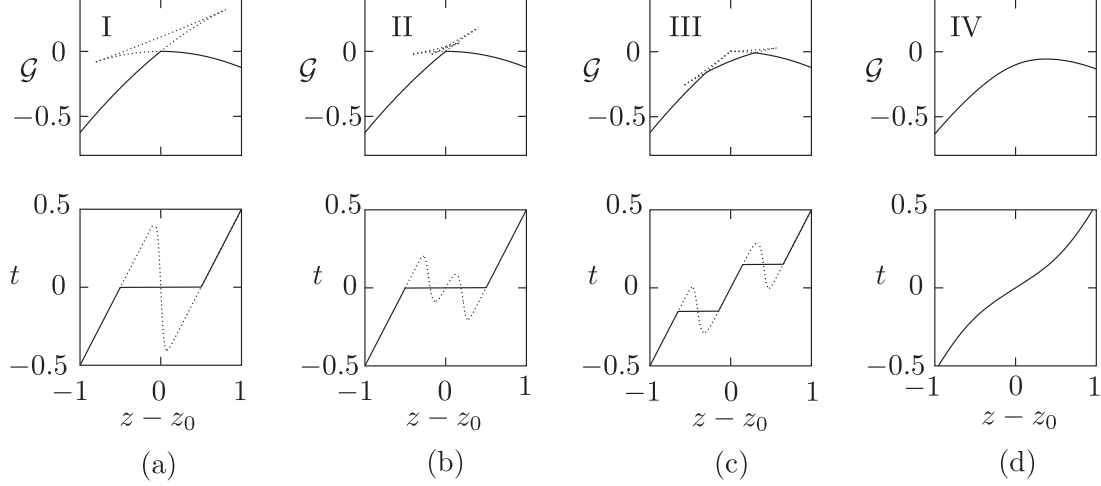


Figure 11. The equilibrium free (Gibbs) energy-strain relation in the soft device and the corresponding tension-strain relation. (a) Phase I: $\lambda_J = 0$, $\beta = 50$; (b) Phase II: $\lambda_J = -0.2$, $\beta = 50$; (c) Phase III: $\lambda_J = -0.4$, $\beta = 50$; and (d) Phase IV: $\lambda_J = -0.2$, $\beta = 4$. Other parameters: $v_0 = 0$. Solid curves correspond to ground states, dotted lines show some other stable and unstable equilibria.

The corresponding self-consistency relation defining the equilibrium value of the order parameter reads,

$$\phi_* = \frac{\sinh \frac{\beta\phi_*}{4}}{\sqrt{e^{-\beta\lambda_J} + \sinh^2 \frac{\beta\phi_*}{4}}}. \quad (21)$$

Near the second-order phase transition we can expand the free energy \mathcal{G} for small ϕ in Taylor series. Leaving only the first terms we obtain $\tilde{\mathcal{G}}(\beta, \phi) = a_0 + a_2\phi^2 + a_4\phi^4$ where,

$$a_0 = \frac{1}{8} - \frac{\log(\sqrt{e^{-\beta\lambda_J} + 1})}{\beta}, a_2 = \frac{1}{8} - \frac{\beta}{32\sqrt{e^{-\beta\lambda_J}}}, a_4 = \frac{\beta^3(3e^{\beta\lambda_J} - 1)}{6144\sqrt{e^{-\beta\lambda_J}}}. \quad (22a)$$

The critical inverse temperature, β_c is such that the second order term in the expansion vanishes, hence it must solve the equation $32\sqrt{e^{-\beta_c\lambda_J}} = 8\beta_c$. In the limit case were $\lambda_J \rightarrow 0$ we obtain $\beta_c = 4$ which agrees with the corresponding expression in the hard device ensemble when $\lambda_f = 0$.

To locate the tricritical point (TCP) we need to extend our Landau type expansion to the sixth-order. We obtain $\tilde{\mathcal{G}}(\beta, \phi) = a_0 + a_2\phi^2 + a_4\phi^4 + a_6\phi^6$ where the new coefficient is

$$a_6 = \frac{\beta^5(30e^{\beta\lambda_J} - 45e^{2\beta\lambda_J} - 1)}{2949120\sqrt{e^{-\beta\lambda_J}}}. \quad (23)$$

Putting to zero the second and the fourth term in this expansion we obtain two equations $\beta = 4e^{-\beta\lambda_J/2}$, and $e^{-\beta\lambda_J/2} = \sqrt{3}$. The tricritical point TCP is then located at $\beta_{TCP} = 4\sqrt{3}$ and $\lambda_{JTCP} = -\log 3/4\sqrt{3}$. The first-order transition line is obtained by requiring that $\mathcal{G}(\beta, \phi = 0) = \mathcal{G}(\beta, \phi = \phi_*)$, where

$$\phi_* = \pm \sqrt{\frac{-a_4 + \sqrt{a_4^2 - 3a_2a_6}}{3a_6}}, \quad (24)$$

We can now build the full phase diagram in the 3D space $(\lambda_J, \lambda_f, \beta)$. Phase II and IV with $\phi = 0$ from Phase I and II where $\phi \neq 0$, see Fig. 12. We assume that the system is in the stall state which means $z = z_0$ in the hard device and $t = 0$ in the soft device ensemble.

In the phase diagram Fig. 12 (a) the plane $\lambda_f = 0$ describe the soft device ensemble while any other plane $\lambda_f = \text{const} > 0$ correspond to ensembles with different rigidity of the hard device. The (blue) surface separates the

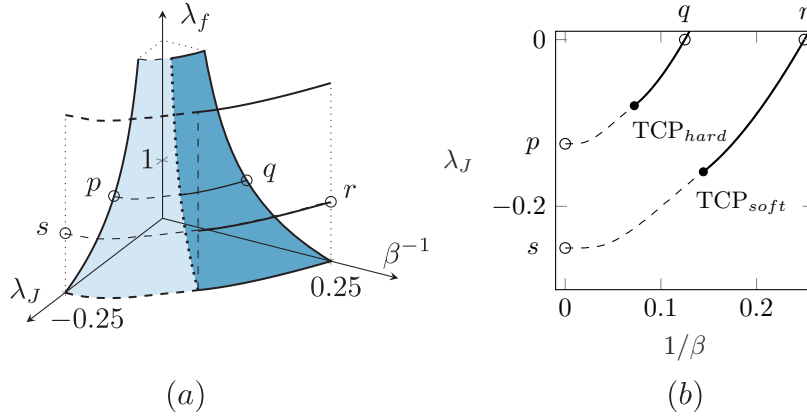


Figure 12. (a) Phase diagram in the 3D space $(\lambda_J, \lambda_f, \beta^{-1})$ for the case of hard device (colored surface, dark blue-second order phase transition, light blue-first order phase transition). The soft device phase diagram is shown by a transparent vertical cylindrical surface (b) Section of both phase diagrams in (a). For the case of a hard device, we fixed the value of parameter $\lambda_f = 1$.

domain of stability of Phases III and IV from the domain of stability of Phases I and II. In this representation, the phase boundary evolves with rigidity λ_f producing one parametric family of ensembles. A comparison of the sections $\lambda_f = 0$ (soft) and $\lambda_f = 1$ (typical hard) is presented in Fig. 12 (b) showing, for instance, that the location of the tricritical points in these two ensembles is different. Since for each half sarcomere, the value of the lump elasticity λ_f may vary with perpetual re-configuring of the surrounding effective matrix, the location of the actual tricritical point can be considered as floating.

The presence, in the phase diagram of the system, of the two closely located critical lines that terminate in the two tricritical points may contribute to the system's ability to perform robustly and might be, in this sense, functional. Previously we have shown that such double criticality may actualize in the system of muscle cross-bridges due to quenched disorder [28]. Here we neglect the quenched disorder, which, of course, also contributes to the destabilization of the coherent response, and focus instead on steric antiferromagnetic interaction as the main factor preventing strongly cooperative response. The importance of the fact that the near-criticality condition is achieved in both soft and hard device ensembles almost concomitantly stems from the mixed nature of the loading conditions experienced by a single half sarcomere. We recall that muscle architecture involves both parallel and series connections. Parallel elements respond to a common displacement (hard device, Helmholtz ensemble), while series structures sense a common force (soft device, Gibbs ensemble). The dominance of long-range interactions induces different collective behavior in force and length controlled ensembles and to ensure the robustness of the response under a broad range of mechanical stimuli, the system can benefit from being poised in the vicinity of both types of critical regimes.

Note also that throughout this paper we have been assuming that the stiffness $\lambda_f = \kappa_f/N$ is a size-independent constant. Therefore we implicitly assumed that $\kappa_f \sim N$. We recall that the (macroscopic) stiffness κ_f represents elastic filaments which support a parallel bundle of N crossbridges. An alternative assumption would be that filaments are not stiffer than cross-bridges and therefore κ_f is N independent, see for instance [28]. In this case $\lambda_f \sim 1/N$, and the number of crossbridges N become a control parameter in the phase diagram. This means that an active control of the number of attached myosin heads could induce a structural change in the overall mechanical response of the system. For instance, it was shown that the fraction of myosin motors attached in the OFF state (heads folded back toward the M-line) depends on the thick filament stress [60]. The time course of the change in conformation of the population of myosin motors in a half-sarcomere was also traced by quick freezing of a single muscle fiber and by using cryo-EM [61]. Such modulation of the number of attached crossbridges may be an indication of an active control, however, the theoretical exploration of this idea will not be pursued in this paper.

ANTIFERROMAGNETIC ORDER

Note that the order parameter ϕ , which is the mechanical analog of magnetization, cannot differentiate between phases I and II when $\phi \neq 0$ and III and IV when $\phi = 0$. Finer features of the local spin distribution can be captured if we introduce parameter distinguishing between ferromagnetic and antiferromagnetic spins' arrangements.

We recall that in magnetism, the system is antiferromagnetic if it is energetically favorable for neighboring spins to align in opposite directions. In the simplest antiferromagnets, the crystal may be divided into two sublattices, A and B, so that if the spins occupying one sublattice point one way, those occupying the other, point the opposite way so that the spins of nearest-neighbor atoms are always antiparallel [62, 63]. Since the net magnetization is equal to zero in such a state, the order parameter ϕ cannot distinguish between paramagnetic (our Phase IV) and antiferromagnetic (our Phase III) phases.

To obtain an approximate picture of the transition to antiferromagnetic behavior we employ a two-sublattice mean-field approximation [44, 64, 65]. We first introduce the conventional spin variable $s_i = 2x_i + 1$, so that $s_i = \pm 1$, then distinguish magnetizations in different sublattices introducing $\phi_a = \langle s_{i \in A} \rangle = (2/N) \sum_{i \in A} s_i$, and $\phi_b = \langle s_{i \in B} \rangle = (2/N) \sum_{i \in B} s_i$. Then the *staggered* magnetization can be defined as $\phi_s = (\phi_a - \phi_b)/2$, while $\phi = (\phi_a + \phi_b)/2$.

If we express the Hamiltonian (3) in terms of the spin variables, $s_i = \pm 1$ the relaxed energy can be written as,

$$E(s_i, z) = -\frac{1}{8N(1+\lambda_f)} \sum_{i,j} s_i s_j - \frac{\lambda_J}{4} \sum_i s_i s_{i+1} - h(z) \sum_i s_i + f(z). \quad (25)$$

where

$$h(z) = \frac{2\lambda_f z - 1}{4(1+\lambda_f)} + \frac{1}{4} - \frac{v_0}{2} + \frac{\lambda_J}{2}, \quad f(z) = \sum_i \frac{\lambda_f z(1+z)}{2(1+\lambda_f)} + \frac{1}{4} + \frac{v_0}{2} - \frac{1}{8(1+\lambda_f)} + \frac{\lambda_J}{4}.$$

This energy can be subdivided into two lattices (A and B) and in the mean-field approximation we can express the values of spins on the corresponding sublattices as $\phi_{a,b} + \tilde{s}_{i \in A,B}$, where $\phi_{a,b}$ are the average values and the fluctuations $\tilde{s}_{i \in A,B}$ are considered to be small. Then, we obtain the approximate Hamiltonian

$$\begin{aligned} \mathcal{H}_{mf} = & -\frac{1}{8N(1+\lambda_f)} \sum_{i,j} (\phi_a + \tilde{s}_{i \in A} + \phi_b + \tilde{s}_{i \in B})(\phi_a + \tilde{s}_{j \in A} + \phi_b + \tilde{s}_{j \in B}) \\ & - \frac{\lambda_J}{4} \sum_{\langle i,j \rangle} (\phi_a + \tilde{s}_{i \in A} + \phi_b + \tilde{s}_{i \in B})(\phi_a + \tilde{s}_{j \in A} + \phi_b + \tilde{s}_{j \in B}) \\ & - h(z) \sum_{i \in A} (\phi_a + \tilde{s}_{i \in A}) - h(z) \sum_{i \in B} (\phi_b + \tilde{s}_{i \in B}) + f(z), \end{aligned} \quad (26)$$

where the notation $\langle i, j \rangle$ indicates that i and j are nearest neighbors. We neglect quadratic terms in the fluctuation, then the problem is posed for $s_{i \in A,B}$, by substituting $\tilde{s}_{i \in A,B} = s_{i \in A,B} - \phi_{a,b}$,

$$\mathcal{H}_{mf} = NJ_{eff} \phi_a \phi_b + h_a(z) \sum_{i \in A} s_i + h_b(z) \sum_{i \in B} s_i + c(z), \quad (27)$$

where

$$J_{eff} = \frac{1}{4} \left(\frac{1}{\lambda_f + 1} + 2\lambda_J \right)$$

is the effective (mean-field) coupling, which depends on both short- and long-range interactions. The loading dependent effective fields are $h_a(z) = -\phi_b J_{eff} - h_s(z)$ and $h_b(z) = -\phi_a J_{eff} - h_s(z)$, with

$$h_s(z) = \frac{2\lambda_f z - 1}{4(1+\lambda_f)} + \frac{1}{4} - \frac{v_0}{2} + \frac{\lambda_J}{2}.$$

Finally, the additive constant is $c(z) = \frac{N\lambda_f z^2}{2(1+\lambda_f)} + Nv_0$. Using the self-consistency conditions $\phi_{a,b} = \langle \sum_{i \in A,B} s_i \rangle$ we obtain the nonlinear algebraic equations for $\phi_{a,b}$:

$$\begin{aligned} \phi_a &= \frac{1}{\mathcal{Z}_{mf}} \sum_{\{s_i\}} s_{i \in A} e^{-\beta \mathcal{H}_{mf}} = \tanh \beta (J_{eff} \phi_b + h_s) \\ \phi_b &= \frac{1}{\mathcal{Z}_{mf}} \sum_{\{s_i\}} s_{i \in B} e^{-\beta \mathcal{H}_{mf}} = \tanh \beta (J_{eff} \phi_a + h_s) \end{aligned} \quad (28)$$

where $\mathcal{Z}_{mf} = 2^N e^{-N\beta J_{eff} \phi_a \phi_b} (\cosh \beta h_a \cosh \beta h_b)^{N/2}$. The system (28) has a unique solution $\phi_a = \phi_b = 0$ for $\beta \leq \beta_N = -1/J_{eff}$, and acquires two additional nonzero solutions for $\beta > \beta_N$. The analog of stall state in this mean-field problem is $z = z_0^s = (1 + 1/\lambda_f)(v_0 - \lambda_J) - 1/2$. The phase diagram at $z = z_0^s$ is presented in Fig. 13 where we set for simplicity that $v_0 = 0$ and $\lambda_f = 1$.

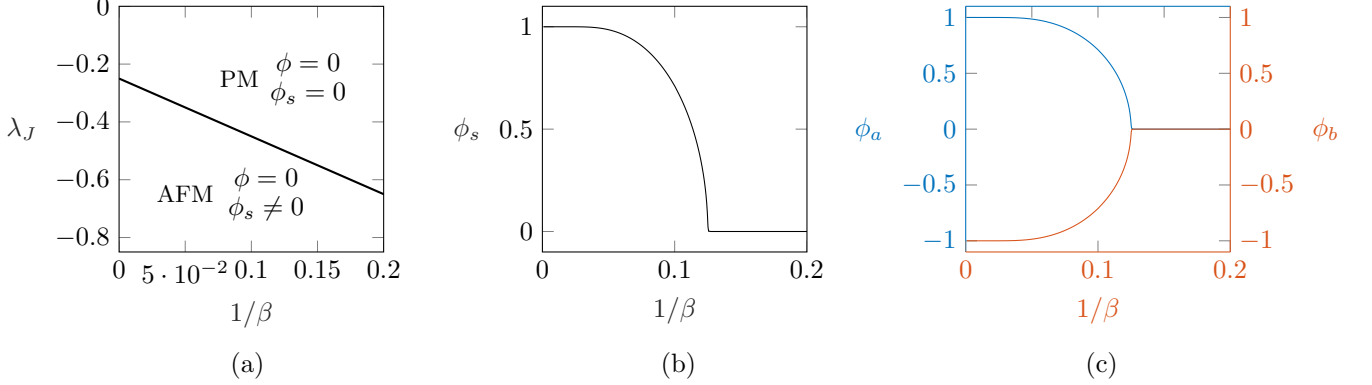


Figure 13. (a) Phase diagram of a model mean-field system in a hard device showing the boundary separating domains with different patterning of spins (representing pre- and post-power stroke configurations of the myosin heads). In the paramagnetic (PM) domain spins are disordered, in the antiferromagnetic (AFM) domain spins are ordered (interdigitated). The loading parameter is fixed at $z = z_0^s$. (b) Staggered magnetization ϕ_s as a function of the non-dimensional temperature $1/\beta$. (c) Order parameters for the AFM phase $\phi_{a,b}$ as functions of $1/\beta$. Other parameters: $\lambda_J = -0.5$.

Since we neglected the crucial long-range interactions in our system due to myosin backbones and treated the steric short-range interactions only at the mean-field level, the resulting phase diagram in Fig. 13(a) is too oversimplified to capture our four Phases I, II, III, IV. The only division which can be illustrated in this way is between the paramagnetic (PM) phase IV and antiferromagnetic (AFM) phase III. The corresponding line on the plane $(\lambda_J, 1/\beta)$ clearly shows that the AFM phase is favored by low temperatures and strong negativity of the coupling constant λ_J .

To reveal the antiferromagnetic ordering emerging in Phases II and III, we can also characterize the two-point correlation function directly $G(i, i+j) = \langle x_i x_j \rangle - \langle x_i \rangle \langle x_j \rangle$ in the hard device ensemble by using again the transfer matrix method. Following [55], we write

$$\langle x_i \rangle = \frac{1}{\mathcal{Z}} \int dy \sum_{\{x\}} e^{-\beta E(x_i, y, z)} x_i = \frac{1}{\mathcal{Z}} \int dy e^{-N\beta\varphi(y, z)} \sum_{x_i} \dots \sum_{x_N} [\mathbf{T}_{x_1 x_2} \mathbf{T}_{x_2 x_3} \dots \mathbf{T}_{x_{i-1} x_i} x_i \mathbf{T}_{x_i x_{i+1}} \dots] \quad (29)$$

Note that the matrix $\sum_{x_i} \mathbf{T}_{x_{i-1} x_i} x_i \mathbf{T}_{x_i x_{i+1}}$ can be equivalently written as $\mathbf{A} = \mathbf{T} \mathbf{X} \mathbf{T}$, where $\mathbf{X} = \begin{pmatrix} 0 & 0 \\ 0 & -1 \end{pmatrix}$ and therefore $\langle x_i \rangle = \frac{1}{\mathcal{Z}} \int dy e^{-N\beta\varphi(y, z)} \text{Tr}(\mathbf{X} \mathbf{T}^N)$, However $\mathbf{T} = \mathbf{S} \mathbf{T}' \mathbf{S}^{-1}$, where \mathbf{T}' is a diagonal matrix with eigenvalues, given by Eq. (7). Then $\langle x_i \rangle = \frac{1}{\mathcal{Z}} \int dy e^{-N\beta\varphi(y, z)} \text{Tr}[\mathbf{S}^{-1} \mathbf{X} \mathbf{S} (\mathbf{T}')^N]$. We can explicitly compute the eigenvectors of \mathbf{T} , $V_{\pm} = (\alpha_{\pm}, 1)$, where $\alpha_{\pm} = e^{\frac{\beta J}{2}} [-\sinh h \pm \sqrt{e^{-\beta J} + \sinh^2 h}]$, so $\mathbf{S} = \begin{pmatrix} \alpha_+ & \alpha_- \\ 1 & 1 \end{pmatrix}$, and

$$\mathbf{S}^{-1} \mathbf{X} \mathbf{S} = \begin{pmatrix} \chi_{11} & \chi_{12} \\ \chi_{22} & \chi_{22} \end{pmatrix} \equiv \begin{pmatrix} -\frac{\sinh h}{2\sqrt{\sinh^2 h + e^{-\beta J}}} - \frac{1}{2} & \frac{e^{-\frac{\beta J}{2}}}{2\sqrt{\sinh^2 h + e^{-\beta J}}} \\ \frac{e^{-\frac{\beta J}{2}}}{2\sqrt{\sinh^2 h + e^{-\beta J}}} & \frac{\sinh h}{2\sqrt{\sinh^2 h + e^{-\beta J}}} - \frac{1}{2} \end{pmatrix}. \quad (30)$$

Then using Laplace method and the fact that $\lim_{N \rightarrow \infty} (\lambda_2/\lambda_1)^N \rightarrow 0$, we obtain

$$\langle x_i \rangle = \chi_{11} = -\frac{\sinh h}{2\sqrt{\sinh^2 h + e^{-\beta J}}} - \frac{1}{2}. \quad (31)$$

The two-point correlation function can be compute similarly. Note first that

$$\langle x_i x_j \rangle = \frac{1}{Z} \int dy e^{-N\beta\varphi(y,z)} \text{Tr} \left[(S^{-1} \mathbf{X} \mathbf{S}) (\mathbf{T}')^j (S^{-1} \mathbf{X} \mathbf{S}) (\mathbf{T}')^{N-j} \right] \quad (32)$$

Again, in the limit $N \rightarrow \infty$, we obtain $\langle x_i x_j \rangle = \chi_{11}^2 + \chi_{12}\chi_{21} (\lambda_2/\lambda_1)^j$, which allows us to finally write

$$G(i, i+j) = \langle x_i x_j \rangle - \langle x_i \rangle \langle x_j \rangle = \chi_{12}\chi_{21} \left(\frac{\lambda_2}{\lambda_1} \right)^j = \frac{1}{4 + 4 e^{\beta J} \sinh^2 h} \left[\frac{\cosh h - \sqrt{e^{-\beta J} + \sinh^2 h}}{\cosh h + \sqrt{e^{-\beta J} + \sinh^2 h}} \right]^j. \quad (33)$$

Here $h = \frac{\beta}{2}(y_* + 1/2 - v_0)$, and y_* is given by (10). To illustrate (33) it is convenient to use the spin variables $s_i = \pm 1$ defined by $2x_i = s_i - 1$. In Fig. 14 we show the function $G_s(j) \equiv G_{s_i}(i, i+j) = 4G_{x_i}(i, i+j)$ which clearly distinguished between the ferromagnetic (FM) and antiferromagnetic (AFM) phases; note that we do not attempt here to directly associate these regimes with the phases defined in the Fig. 7.

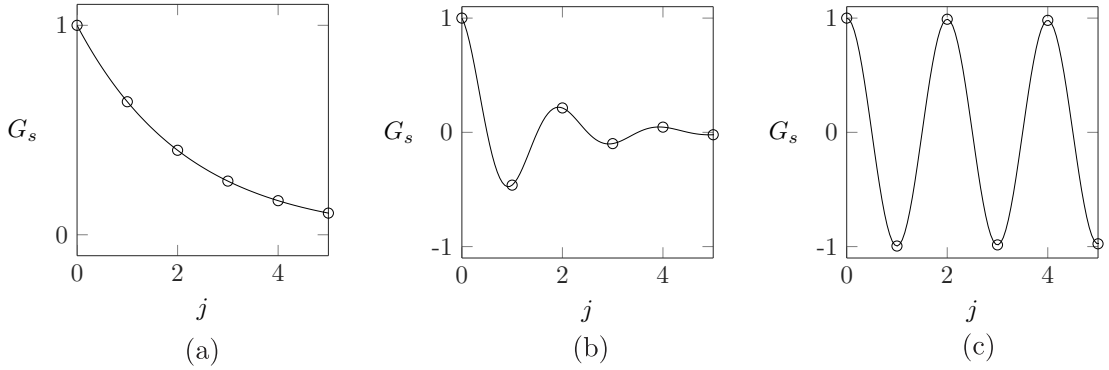


Figure 14. Two-point correlation function in different phases for the model system, see Fig. 13(a). The loading parameter is fixed at $z = z_0$. Other parameters: (a) $\beta = 20$, $\lambda_J = 0.1$ PM-phase; (b) $\beta = 10$, $\lambda_J = -0.2$ PM-phase; (c) $\beta = 20$, $\lambda_J = -0.5$ AFM-phase.

To summarize, we have shown if short-range steric interactions between cross-bridges of antiferromagnetic type are sufficiently strong, then the state of isometric contractions is not only mechanically stable in the sense that it has positive stiffness, but it is also ordered in the way that exactly half of the cross-bridges is in pre-power stroke state and another half in the post-power stroke state, moreover the conformation states oscillate at lattice scale so that both conformations are effectively present at any location inside a half-sarcomere.

TWO HALF-SARCOMERES

In this section, we show how the presence of antiferromagnetic short-range interactions allows the system to avoid instability developing into macroscopic inhomogeneity. One can say that to maintain homogeneity at the macroscale such system chooses to be maximally inhomogeneous at the microscopic scale.

So far, we have been dealing with a single half-sarcomere behavior, which is the basic unit of contraction. Even having non-convex elastic energy and negative stiffness, such a unit is still stable in a hard device. This case's instability comes when more than one element with non-convex energies is loaded in a hard device while being arranged in series. Even if the system includes only two units like this, they do not need to deform in an affine way and can accept instead different deformational states.

This is an important issue since muscle fiber is often represented as a series of connections of half-sarcomeres. It has been shown that if the energy of individual half-sarcomeres is non-convex such association breaks into macroscopic islands of either fully pre- or fully post-power stroked half-sarcomeres [19, 21]. Such instability would be prevented if the energy of a half sarcomere is convexified in the stall configuration. As we have shown in the previous sections, such convexification occurs when the system is either in Phase IV or Phase III. It has been already known to Huxley that the first option is not viable in view of insufficiently high reduced temperature in physiological conditions. That

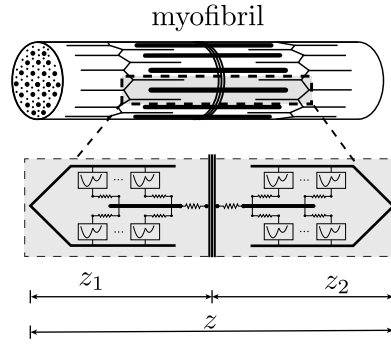


Figure 15. Schematic representation of a single sarcomere. Inset illustrate the equivalent mechanical model: two half-sarcomeres connected in series.

is why we consider below the only low-temperature option when the destabilizing steric short-range interactions are sufficiently strong, and the physiological system is in Phase III.

To illustrate the disappearance of the macroscopic instability in this case it is sufficient to consider the simplest system with only two half-sarcomeres connected in series. Such system can be viewed as a prototypical description of a single sarcomere, see Fig. 15. Experiments suggests that in stall conditions each sarcomere contains a macroscopically (but not necessarily microscopically) uniform mixture of pre- and post-power stroke cross-bridges [30].

Suppose that each half sarcomere is equilibrated independently at the microscale and therefore behaves at the macroscale according to the elastic constitutive relation generated by the free energy $\mathcal{F}(\beta, z)$, see (9). We can then write the equilibrium energy of the whole system loaded in a hard device in the form,

$$\mathcal{F}_2(\beta, z, z_1) = \mathcal{F}(\beta, z_1) + \mathcal{F}(\beta, z - z_1). \quad (34)$$

where z is the macroscopic controlling parameter. The extra variable z_1 can be eliminated using the equilibrium condition $\partial\mathcal{F}(\beta, z_1)/\partial z_1 = \partial\mathcal{F}(\beta, z - z_1)/\partial z_1$. Substituting the equilibrium value $z_1(\beta, z)$ into (34) we obtain the function $\mathcal{F}_2(\beta, z) = \mathcal{F}_2(\beta, z, z_1(\beta, z))$ and construct the equilibrium force-elongation relation $t(\beta, z) = d\mathcal{F}_2(\beta, z)/dz$. It would be also of interest to compute for each half-sarcomere, the fraction of cross-bridges in either pre- or post-power stroke conformations. For half-sarcomeres 1 and 2, respectively, it will be given by the functions

$$\phi_{1,2}(\beta, z) = 2(\lambda_f + 1)y_*^{1,2}(\beta, z) - 2\lambda_f z + 1 \quad (35)$$

where the function $y_*(\beta, z)$ is given by (10).

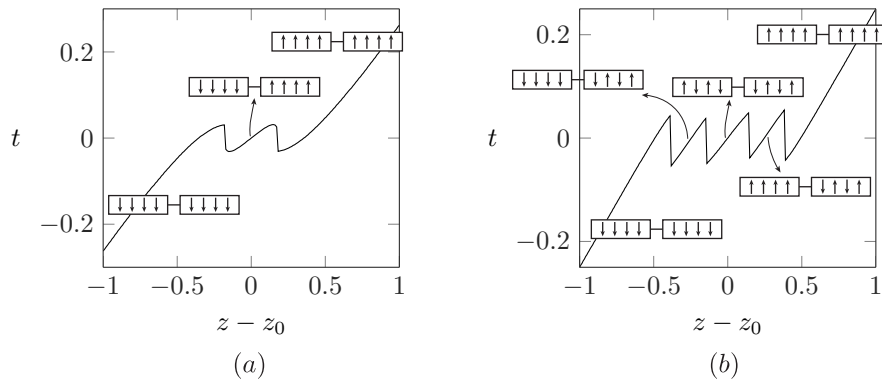


Figure 16. Mechanical response of the system consisting of two half-sarcomere units connected in series with each half-sarcomere represented by infinite number of cross-bridges (thermodynamic limit). Solid curves show the equilibrium tension elongation curves, the insets illustrate the associated configurations of cross-bridges. Parameters: (a) $v_0 = 0$, $\beta = 5$, $\lambda_f = 1$, and $\lambda_J = 0$ (no short-range interactions). (b) $v_0 = 0$, $\beta = 25$, $\lambda_f = 1$, and $\lambda_J = -0.25$, (strong antiferromagnetic short-range interactions).

In Fig. 16 and Fig. 17 we compare the response of two half-sarcomeres in series depending on whether their constitutive response follows the one from Phase I, see Fig. 16(a) or Phase III, see Fig. 16(b).

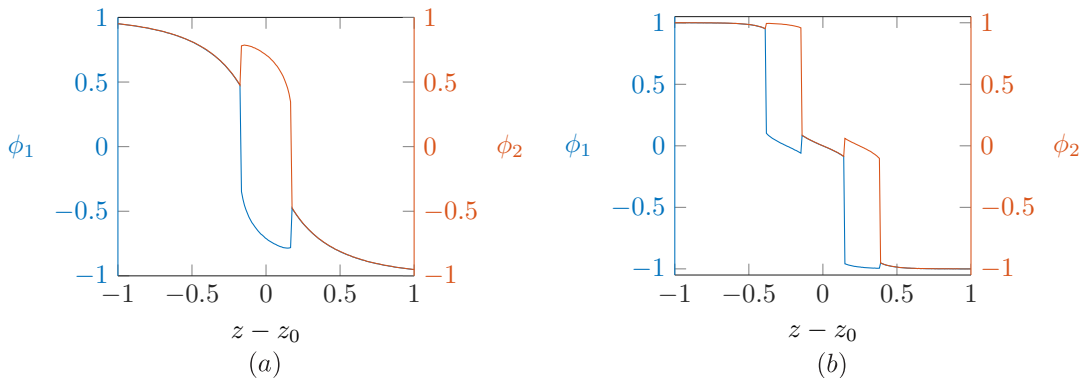


Figure 17. Strain response of the 'local' order parameters for the system of two half-sarcomeres connected in series. The colored curves show ϕ_1 and ϕ_2 are the order parameter of the individual half-sarcomeres. Parameters: (a): $v_0 = 0$, $\beta = 5$, $\lambda_f = 1$, and $\lambda_J = 0$ (no short-range interactions); b) $v_0 = 0$, $\beta = 25$, $\lambda_f = 1$, and $\lambda_J = -0.25$ (strong antiferromagnetic short-range interactions).

If short-range interactions are of *ferromagnetic* type and the individual subsystems are in Phase I, we observe that while the effective stiffness in the stall state $z = z_0$ is positive, see Fig. 16(a), the macro-state is non-affine with ϕ_1 and ϕ_2 taking different values. This means that the two half-sarcomeres in series have different internal structures that are both pure: one is fully in pre-power stroke state and another one is fully in post-power stroke state, see Fig. 17(a).

If instead, the short-range interactions are of *antiferromagnetic* type and the individual half-sarcomeres are in Phase III, the whole sarcomere (in stall conditions) has positive stiffness, see Fig. 16(b), and its macro-configuration is affine with the order parameters ϕ_1 and ϕ_2 taking the same value, see Fig. 17(b). This means that the two half-sarcomeres in series have the same internal structure, which is, however, micro-inhomogeneous, with cross-bridges equally divided between pre- and post-power stroke conformations.

Outside a neighborhood of the stall state, the system with *ferromagnetic* type short-range interactions is microscopically homogeneous with all half sarcomeres occupying the same pure state. Instead, the system with *antiferromagnetic* type interactions develops two zones of non-affine behavior where one of the two half sarcomeres is in a pure state while the other one is in a mixed state.

This simplified description can be immediately extended to cover the case of N half-sarcomeres connected in series. In the case of dominating antiferromagnetic interactions, the stall state will remain mechanically stable, macroscopically homogeneous, and microscopically inhomogeneous. Outside the stall state's immediate vicinity, there will be different regimes with a variable number of coexisting half-sarcomeres in a pure and mixed state. The overall macroscopic force-elongation curve will then be wavy with an overall slightly positive average slope as observed in experiments. In the limit $N \rightarrow \infty$, we obtain weak convergence to an apparently stress-strain curve whose local microscopic derivative is nevertheless different from its macroscopic (averaged) value.

CONCLUSIONS

We presented a mathematical model describing the passive mechanical response of tetanized muscle fibers, which is relevant for the analysis of experiments involving fast mechanical perturbations imposed on the state of isometric contractions. The observed overall homogeneity of such response was previously shown to be incompatible with the most basic theoretical modeling. In particular, it was previously concluded that not only the classical model of Huxley-Simmons [1] but also its more recent generalizations [4], require that all cross-bridges inside a half-sarcomere should be either in pre- or in post-power stroke states.

The standard HS type model assumes that the bi-stable nature of myosin heads can be modeled by spin variables and that inside a single half-sarcomere, the myosin cross-bridges are arranged in parallel [5, 38]. This parallel structure is responsible for mean-field type interaction among different cross-bridges, which forces them to act synchronously. To compromise the coherent response of such parallel bundles, we had to move beyond the HS framework [20] and introduce into the model the antiferromagnetic mechanical interactions between neighboring cross-bridges. We then

studied the competition between these destabilizing short-range interactions and the stabilizing long-range interactions of HS. We showed that while an increase in the strength of the ferromagnetic short-range interactions ($\lambda_J > 0$) would have the same effect as a decrease of temperature, leaving the overall qualitative behavior of HS unchanged, the presence of antiferromagnetic interactions ($\lambda_J < 0$) drastically changes the qualitative behavior of the system. The main effect is that by tuning the parameter $\lambda_J < 0$ one can introduce a new energy well corresponding the stall state and in this way stabilize the state of isometric contractions. At a fixed strength of long-range interactions (fixed λ_f), the phase diagram in (β, λ_J) space, shows a line of second-order phase transition which expands the critical regime found in [20] for the special case $\lambda_J = 0$.

The proposed model shows that to make a macroscopically homogeneous response possible the system must be microscopically inhomogeneous. Micro-inhomogeneity, achieved by activating short-range interactions of antiferromagnetic type, takes the form of periodic interdigitated patterns with neighboring sarcomeres taking alternatively either pre- or post-power stroke conformations. Such patterns replace the highly coherent micro-homogeneous mechanical response favored by the original HS model. The predicted micro-inhomogeneity may be beneficial as it breaks the coherency of the response and facilitates the swift transition to either fully pre- or fully post-power stroke configuration in response to external excitation. We also argue that evolution could use short-range interactions to tune the muscle machinery to perform near the conditions of "double criticality", where both the Helmholtz and the Gibbs free energies are singular. Such design would be highly functional given that elementary force-producing units are expected to perform in a mixed soft-hard device.

ACKNOWLEDGMENTS

The authors thank Marco Linari and Matthieu Caruel for helpful discussions. H.B.R. was supported by a PhD fellowship from Ecole Polytechnique; L. T. was supported by the grant ANR-10-IDEX-0001-02 PSL.

* hudson.borja-da-rocha@polytechnique.edu

† lev.truskinovsky@espci.fr

- [1] A. F. Huxley and R. M. Simmons, *Nature* **233**, 533 (1971).
- [2] R. J. Podolsky, *Nature* **188**, 666 (1960).
- [3] T. L. Hill, *Progress in Biophysics and Molecular Biology* **28**, 267 (1974).
- [4] M. Caruel and L. Truskinovsky, *Reports on Progress in Physics* **81**, 036602 (2018).
- [5] G. Piazzesi, M. Reconditi, M. Linari, L. Lucii, Y.-B. Sun, T. Narayanan, P. Boesecke, V. Lombardi, and M. Irving, *Nature* **415**, 659 (2002).
- [6] G. Piazzesi, M. Reconditi, M. Linari, L. Lucii, P. Bianco, E. Brunello, V. Decostre, A. Stewart, D. Gore, T. Irving, M. Irving, and V. Lombardi, *Cell* **131**, 784 (2007).
- [7] M. Irving, V. Lombardi, G. Piazzesi, and M. A. Ferenczi, *Nature* **357**, 156 (1992).
- [8] R. Sheshka and L. Truskinovsky, "Power-stroke-driven muscle contraction," in *The Mathematics of Mechanobiology: Cetraro, Italy 2018*, edited by D. Ambrosi and P. Ciarletta (Springer International Publishing, Cham, 2020) pp. 117–207.
- [9] H. Borja da rocha, *Collective effects in muscle contraction and cellular adhesion*, Theses, Université Paris-Saclay (2018).
- [10] A. F. Huxley, *Philosophical Transactions of the Royal Society B: Biological Sciences* **355**, 433 (2000).
- [11] L. E. Ford, A. F. Huxley, and R. M. Simmons, *The Journal of physiology* **311**, 219 (1981).
- [12] E. Brunello, M. Reconditi, R. Elangovan, M. Linari, Y. B. Sun, T. Narayanan, P. Panine, G. Piazzesi, M. Irving, and V. Lombardi, *Proceedings of the National Academy of Sciences of the United States of America* **104**, 20114 (2007).
- [13] L. Marcucci and L. Truskinovsky, *Phys. Rev. E* **81**, 051915 (2010).
- [14] L. Marcucci and L. Truskinovsky, *The European Physical Journal E* **32**, 411 (2010).
- [15] M. Caruel and L. Truskinovsky, *Phys. Rev. E* **93**, 062407 (2016).
- [16] M. Caruel, J.-M. Allain, and L. Truskinovsky, *Journal of the Mechanics and Physics of Solids* **76**, 237 (2015).
- [17] E. Brunello, M. Caremani, L. Melli, M. Linari, M. Fernandez-Martinez, T. Narayanan, M. Irving, G. Piazzesi, V. Lombardi, and M. Reconditi, *The Journal of Physiology* **592**, 3881 (2014).
- [18] M. Linari, I. Dobbie, M. Reconditi, N. Koubassova, M. Irving, G. Piazzesi, and V. Lombardi, *Biophysical Journal* **74**, 2459 (1998).
- [19] A. Vilfan and T. Duke, *Biophysical journal* **85**, 818 (2003).
- [20] M. Caruel, J.-M. Allain, and L. Truskinovsky, *Physical Review Letters* **110**, 248103 (2013).
- [21] G. Puglisi and L. Truskinovsky, *Journal of the Mechanics and Physics of Solids* **48**, 1 (2000).
- [22] D. E. Rassier and I. Pavlov, "Contractile characteristics of sarcomeres arranged in series or mechanically isolated from myofibrils," in *Muscle Biophysics: From Molecules to Cells*, edited by D. E. Rassier (Springer New York, New York, NY, 2010) pp. 123–140.

- [23] A. F. Huxley and S. Tideswell, *Journal of Muscle Research & Cell Motility* **17**, 507 (1996).
- [24] S. Wu, J. Liu, M. C. Reedy, R. J. Perz-Edwards, R. T. Tregear, H. Winkler, C. Franzini-Armstrong, H. Sasaki, C. Lucaveche, Y. E. Goldman, M. K. Reedy, and K. A. Taylor, *PloS one* **7**, e39422 (2012).
- [25] R. T. Tregear, M. C. Reedy, Y. E. Goldman, K. A. Taylor, H. Winkler, C. Franzini-Armstrong, H. Sasaki, C. Lucaveche, and M. K. Reedy, *Biophysical Journal* **86**, 3009 (2004).
- [26] M. Reconditi, *Reports on Progress in Physics* **69**, 2709 (2006).
- [27] R. T. Tregear, R. J. Edwards, T. C. Irving, K. J. Poole, M. C. Reedy, H. Schmitz, E. Towns-Andrews, and M. K. Reedy, *Biophysical Journal* **74**, 1439 (1998).
- [28] H. Borja da Rocha and L. Truskinovsky, *Phys. Rev. Lett.* **122**, 088103 (2019).
- [29] R. Sheshka, P. Recho, and L. Truskinovsky, *Phys. Rev. E* **93**, 052604 (2016).
- [30] K. Midde, R. Luchowski, H. Das, J. Fedorick, V. Dumka, I. Gryczynski, Z. Gryczynski, and J. Borejdo, *Biophysical Journal* **100**, 1024 (2011).
- [31] K. Hirose and T. Wakabayashi, *Journal of Muscle Research & Cell Motility* **14**, 432 (1993).
- [32] M. Reedy, *Journal of Cell Science* **113**, 3551 (2000).
- [33] D. D. Thomas, S. Ramachandran, O. Roopnarine, D. W. Hayden, and E. M. Ostap, *Biophysical journal* **68**, 135S (1995).
- [34] D. D. Thomas, S. Ramachandran, O. Roopnarine, D. W. Hayden, and E. M. Ostap, *Biophysical journal* **68**, 135S (1995).
- [35] M. Reconditi, M. Caremani, F. Pinzauti, J. D. Powers, T. Narayanan, G. J. M. Stienen, M. Linari, V. Lombardi, and G. Piazzesi, *Proceedings of the National Academy of Sciences* **114**, 3240 (2017), <https://www.pnas.org/content/114/12/3240.full.pdf>.
- [36] G. Piazzesi, F. Francini, M. Linari, and V. Lombardi, *The Journal of physiology* **445**, 659 (1992).
- [37] M. Reconditi, M. Linari, L. Lucii, A. Stewart, Y.-B. Sun, P. Boesecke, T. Narayanan, R. F. Fischetti, T. Irving, G. Piazzesi, M. Irving, and V. Lombardi, *Nature* **428**, 578 (2004).
- [38] M. Kaya, Y. Tani, T. Washio, T. Hisada, and H. Higuchi, *Nature Communications* **8**, 16036 (2017).
- [39] J. M. Squire, D. M. Paul, and E. P. Morris, “Myosin and actin filaments in muscle: Structures and interactions,” in *Fibrous Proteins: Structures and Mechanisms*, edited by D. A. Parry and J. M. Squire (Springer International Publishing, Cham, 2017) pp. 319–371.
- [40] M. V. Razumova, A. E. Bukatina, and K. B. Campbell, *Biophysical Journal* **78**, 3120 (2000).
- [41] S. M. Mijailovich, J. J. Fredberg, and J. P. Butler, *Biophysical Journal* **71**, 1475 (1996).
- [42] T. L. Daniel, A. C. Trimble, and P. B. Chase, *Biophysical Journal* **74**, 1611 (1998).
- [43] J. F. Nagle, *Phys. Rev. A* **2**, 2124 (1970).
- [44] J. C. Bonner and J. F. Nagle, *Journal of Applied Physics* **42**, 1280 (1971).
- [45] M. Kardar, *Phys. Rev. B* **28**, 244 (1983).
- [46] P. A. Rikvold, G. Brown, S. Miyashita, C. Omand, and M. Nishino, *Phys. Rev. B* **93**, 064109 (2016).
- [47] A. Campa, G. Gori, V. Hovhannisyan, S. Ruffo, and A. Trombettoni, *Journal of Physics A: Mathematical and Theoretical* **52**, 344002 (2019).
- [48] F. Bouchet, S. Gupta, and D. Mukamel, *Physica A: Statistical Mechanics and its Applications* **389**, 4389 (2010), proceedings of the 12th International Summer School on Fundamental Problems in Statistical Physics.
- [49] J. Barré, D. Mukamel, and S. Ruffo, *Phys. Rev. Lett.* **87**, 030601 (2001).
- [50] J. Barré, D. Mukamel, and S. Ruffo, “Ensemble inequivalence in mean-field models of magnetism,” in *Dynamics and Thermodynamics of Systems with Long-Range Interactions*, edited by T. Dauxois, S. Ruffo, E. Arimondo, and M. Wilkens (Springer Berlin Heidelberg, Berlin, Heidelberg, 2002) pp. 45–67.
- [51] L. Marcucci and C. Reggiani, *Frontiers in Physiology* **7**, 1 (2016).
- [52] L. Marcucci, T. Washio, and T. Yanagida, *PLoS Computational Biology* **12**, 1 (2016).
- [53] M. Ostilli and F. Mukhamedov, *Physica A* **555**, 124415 (2020).
- [54] J. Yeomans, *Statistical Mechanics of Phase Transitions* (Clarendon Press, 1992).
- [55] N. Goldenfeld, *Lectures on phase transitions and the renormalization group*, *Frontiers in physics* (Addison-Wesley, Advanced Book Program, 1992).
- [56] While it would have been more realistic to assume that this ratio is around 70-30 [66], we have chosen to present our results only in the most simple setting that can be easily corrected by the appropriate adjustment of the parameter v_0 .
- [57] K. Christensen and N. R. Moloney, *Complexity and criticality*, Vol. 1 (World Scientific Publishing Company, 2005).
- [58] R. Pathria and P. Beale, *Statistical Mechanics* (Elsevier Science, 1996).
- [59] A. Campa, T. Dauxois, and S. Ruffo, *Physics Reports* **480**, 57 (2009).
- [60] M. Linari, E. Brunello, M. Reconditi, L. Fusi, M. Caremani, T. Narayanan, G. Piazzesi, V. Lombardi, and M. Irving, *Nature* **528**, 276 (2015).
- [61] K. A. Taylor, H. Schmitz, M. C. Reedy, Y. E. Goldman, C. Franzini-Armstrong, H. Sasaki, R. T. Tregear, K. Poole, C. Lucaveche, R. J. Edwards, L. F. Chen, H. Winkler, and M. K. Reedy, *Cell* **99**, 421 (1999).
- [62] J. Crangle, *Solid State Magnetism* (Springer Science & Business Media, 2012).
- [63] A. A. Zvyagin and G. A. Skorobogat'ko, *Low Temperature Physics* **32**, 644 (2006).
- [64] R. Agra, F. van Wijland, and E. Trizac, *European Journal of Physics* **27**, 407 (2006).
- [65] P. A. Rikvold, G. Brown, S. Miyashita, C. Omand, and M. Nishino, *Phys. Rev. B* **93**, 064109 (2016).
- [66] M. Irving, G. Piazzesi, L. Lucii, Y.-B. Sun, J. J. Harford, I. M. Dobbie, M. A. Ferenczi, M. Reconditi, and V. Lombardi, *Nature Structural Biology* **7**, 482 (2000).